

# Fast Computation of the Ambiguity Function and the Wigner Distribution on Arbitrary Line Segments

Ahmet Kemal Özdemir, *Student Member, IEEE*, and Orhan Arıkan, *Member, IEEE*

**Abstract**—By using the fractional Fourier transformation of the time-domain signals, closed-form expressions for the projections of their auto or cross ambiguity functions are derived. Based on a similar formulation for the projections of the auto and cross Wigner distributions and the well known two-dimensional (2-D) Fourier transformation relationship between the ambiguity and Wigner domains, closed-form expressions are obtained for the slices of both the Wigner distribution and the ambiguity function. By using discretization of the obtained analytical expressions, efficient algorithms are proposed to compute uniformly spaced samples of the Wigner distribution and the ambiguity function located on arbitrary line segments. With repeated use of the proposed algorithms, samples in the Wigner or ambiguity domains can be computed on non-Cartesian sampling grids, such as polar grids.

**Index Terms**—Ambiguity function, fast computation, fractional Fourier transformation, Wigner distribution.

## I. INTRODUCTION

TIME-FREQUENCY signal processing is one of the fundamental research areas in signal processing. The Wigner distribution (WD) plays a central role in the theory and practice of time-frequency signal processing [1]–[10]. Likewise, the ambiguity function (AF), which is the two-dimensional (2-D) Fourier transform of the Wigner distribution, plays a central role in time-frequency signal analysis [11]–[13] and radar and sonar signal processing [14]–[17].

Because of the availability of efficient computational algorithms, both the WD and AF are usually computed on Cartesian grids [1], [18], [19]. In this paper, by using the fractional Fourier transformation of the time-domain signals, closed-form expressions for the projections of their auto or cross ambiguity functions are derived. Based on a similar formulation for the projections of the auto and cross Wigner distributions [20] and the well-known 2-D Fourier transformation relationship between the ambiguity and Wigner domains, novel closed-form expressions are obtained for the slices of both the WD and the AF. By using discretization of the obtained analytical expressions, efficient algorithms are proposed to compute uniformly spaced samples of the WD and the AF located on arbitrary line segments. With repeated use of these algorithms, it is possible to obtain samples of the WD and AF on non-Cartesian grids, such as polar grids that are the natural sampling grids

of chirp-like signals. The ability of obtaining WD and AF samples over polar grids is potentially very useful in various important application areas including time-frequency domain kernel design, multicomponent signal analysis, time-frequency domain signal detection, and particle location analysis in Fresnel holograms [21]–[28].

The organization of the paper is in accordance with the dual nature of the ambiguity function and Wigner distribution. We first provide some preliminaries on these important concepts. In Section III, by using the Radon-Wigner transformation, analytical expressions are derived for the slices of the auto ambiguity functions. Then, by discretizing the obtained analytical expressions, efficient algorithms are presented for the computation of slices of the ambiguity function. In Section IV, we follow a similar development, leading to novel closed-form expressions for the Radon-ambiguity function, and present efficient algorithms for the computation of slices of the Wigner distribution. In Section V, both the analytical and computational results are extended to the *cross* AF and WD. In Section VI, we provide results of simulated applications of the proposed algorithms. Finally, the paper is concluded in Section VII.

## II. PRELIMINARIES ON THE WIGNER DISTRIBUTION AND THE AMBIGUITY FUNCTION

Discrete time-frequency analysis is the primary investigation tool in the synthesis, characterization, and filtering of time-varying signals. Among the alternative time-frequency analysis algorithms, those belonging to the Cohen's class are the most commonly utilized ones. In this class, the time-frequency distributions of a signal  $x(t)$  are given by<sup>1</sup>

$$\text{TF}_x(t, f) = \int \int \int \kappa(\nu, \tau) x(u + \tau/2) x^*(u - \tau/2) \times e^{j2\pi(\nu u - \nu t - \tau f)} du d\nu d\tau \quad (1)$$

where the function  $\kappa(\nu, \tau)$  is called the kernel [4], [29]. Recent research on the time-frequency signal analysis has revealed that signal dependent choice of the kernel helps in localization of the time-frequency components of the signals [11], [21]–[24]. By choosing  $\kappa(\nu, \tau) = 1$ , the most commonly used member of the Cohen's class (the Wigner distribution) is obtained

$$W_x(t, f) \triangleq \int x(t + t'/2) x^*(t - t'/2) e^{-j2\pi f t'} dt'. \quad (2)$$

Because of its nice energy localization properties, the WD has found important application areas. Definition (2) has been gen-

Manuscript received March 29, 1999; revised October 3, 2000. The associate editor coordinating the review of this paper and approving it for publication was Prof. Gregori Vazquez.

The authors are with the Department of Electrical and Electronics Engineering, Bilkent University, Ankara, Turkey (e-mail: kozdemir@ee.bilkent.edu.tr; oarikan@ee.bilkent.edu.tr).

Publisher Item Identifier S 1053-587X(01)00620-1.

<sup>1</sup>All integrals are from  $-\infty$  to  $+\infty$  unless otherwise stated.

eralized to define the cross-Wigner distribution of two signals  $x(t)$  and  $y(t)$  as

$$W_{xy}(t, f) \triangleq \int x(t + t'/2) y^*(t - t'/2) e^{-j2\pi f t'} dt'. \quad (3)$$

The properties of the cross-Wigner distribution have been investigated in detail [1], [2]. Note that  $W_{xx}(t, f) \equiv W_x(t, f)$  holds.

The 2-D inverse Fourier transform (FT) of the WD is called the (symmetric) ambiguity function, and it has found important application areas including time-frequency signal analysis and radar signal processing

$$A_x(\nu, \tau) \triangleq \iint W_x(t, f) e^{j2\pi(\nu t + \tau f)} dt df \quad (4a)$$

$$= \int x(t + \tau/2) x^*(t - \tau/2) e^{j2\pi \nu t} dt. \quad (4b)$$

Similar to the cross-Wigner distribution, the cross-ambiguity function of two signals  $x(t)$ ,  $y(t)$  is defined as

$$A_{xy}(\nu, \tau) \triangleq \int x(t + \tau/2) y^*(t - \tau/2) e^{j2\pi \nu t} dt. \quad (5)$$

As in (4a), the cross-ambiguity function is related to the cross-Wigner distribution through the 2-D inverse Fourier transformation

$$A_{xy}(\nu, \tau) = \iint W_{xy}(t, f) e^{j2\pi(\nu t + \tau f)} dt df. \quad (6)$$

### III. FAST COMPUTATION OF THE AMBIGUITY FUNCTION ON ARBITRARY LINE SEGMENTS

In this section, an efficient algorithm to compute the ambiguity function on uniformly spaced samples along an arbitrary line segment is provided. For the sake of simplicity, a gradual method of presentation is used where we first consider obtaining uniformly spaced samples of the AF on a line segment centered at the origin. Then, we extend this approach to obtain samples on a line segment positioned radially. Finally, we consider the case of an arbitrary line segment. The presentation of the proposed approach will be as follows: First, the well-known projection-slice relationship between the WD and the AF domains will be given. Then, the projections in the WD domain will be related to the fractional Fourier transformation of the signals involved. Finally, the obtained continuous-time relationship will be discretized to allow the use of a fast fractional Fourier transformation algorithm.

#### A. Radon-Wigner Transform

The Radon-Wigner transform (RWT) or Radon transformation of the Wigner distribution has been introduced for the analysis and classification of multicomponent chirp signals in noise. Several authors investigated RWT and some of its applications in multicomponent signal analysis, time-varying filtering, and adaptive kernel design [25], [30]–[33]. The RWT of a function  $x(t)$  is defined as the Radon transform of its WD. Using the geometry in Fig. 1, RWT can be written as

$$P_x(r, \phi) = \int W_x(r \cos \phi - s \sin \phi, r \sin \phi + s \cos \phi) ds \quad (7)$$

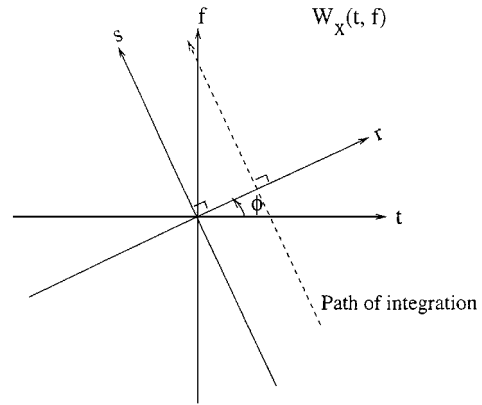


Fig. 1. Radon transform geometry for the RWT.

where  $(r, \phi)$  are the transform domain variables in polar format. With this definition, the RWT can be viewed as the family of the projections  $\{P_x(r, \phi), 0 \leq \phi < \pi\}$ . The projection-slice theorem [34] establishes an important link between the projections of the WD and the slices of the AF. The 1-D inverse Fourier transform of the projection  $P_x(r, \phi)$  with respect to the radial variable  $r$  is the radial slice of the ambiguity function at the angle  $\phi$

$$\int P_x(r, \phi) e^{j2\pi r \lambda} dr = A_x(\lambda \cos \phi, \lambda \sin \phi) \quad (8a)$$

$$= A_x^p(\lambda, \phi) \quad (8b)$$

where  $A_x^p(\lambda, \phi) \triangleq A_x(\lambda \cos \phi, \lambda \sin \phi)$  is the polar representation of the AF. Therefore, once we have the projection  $P_x(r, \phi)$ , we can use the fast Fourier transform (FFT) algorithm to efficiently approximate the samples on the radial slice of the AF. However, to have a practically useful algorithm, we have to obtain the RWT efficiently as well. Fortunately, as it has been shown in [35], the radial slices of the RWT  $[P_x(r, \phi)]$  can be computed directly from the time signal  $x(t)$  by using the fractional Fourier transformation (FrFT)

$$P_x(r, \phi) = |\{\mathcal{F}^a x\}(r)|^2 \equiv |x_a(r)|^2, \quad \text{for } a = \frac{2\phi}{\pi} \quad (9)$$

where  $P_x(r, \phi)$  is the  $\phi$ -Radon projection of the WD given by (7), and  $x_a(r)$  is the  $a$ th-order FrFT of the signal as given in Appendix A. Combining (8) and (9), we obtain the following relation between the AF and the FrFT of a signal:

$$A_x^p(\lambda, \phi) = \int |x_a(r)|^2 e^{j2\pi r \lambda} dr. \quad (10)$$

Thus, the ordinary 1-D inverse Fourier transform of the magnitude squared  $a$ th-order FrFT of a signal is equal to the radial slice of its ambiguity function that makes an angle of  $a\pi/2$  with respect to the  $\nu$  axis in the  $\nu$ - $\tau$  plane.

#### B. Efficient Computation of the Ambiguity Function Samples Along Radial Slices of the Ambiguity Plane

In this section, we provide the details of a fast algorithm for computing radial samples of the ambiguity function. As it will be shown in detail, for an input sequence of length  $N$ , it is possible to compute the samples of AF on an arbitrary line segment

centered at the origin in  $O(N \log N)$  flops.<sup>2</sup> We start with the approximation of the integral in (10) with its uniform Riemann summation. For an equally valid approximation at all angles  $\phi$ , in the rest of this paper, we assume that prior to obtaining its samples,  $x(t)$  is scaled so that its Wigner domain support is approximately confined into a circle with radius  $\Delta_x/2$  centered at the origin. In other words, any  $a$ th-order FrFT of  $x(t)$ , including the signal itself and its ordinary Fourier transform, has negligible energy outside the symmetric interval  $[-\Delta_x/2, \Delta_x/2]$ . For a signal  $x(t)$  with approximate time and frequency supports of  $\Delta_t$  and  $\Delta_f$ , respectively, the required scaling is  $x(t/s)$ , where  $s = \sqrt{\Delta_f/\Delta_t}$  [36].

After the scaling, the double-sided bandwidth of  $|x_a(r)|^2$  is  $2\Delta_x$ . Therefore, its inverse FT given in (10) can be expressed in terms of its uniformly obtained samples at a rate  $2\Delta_x$  using the following discrete-time inverse Fourier transform relation:<sup>3</sup>

$$A_x^p(\lambda, \phi) = \frac{1}{2\Delta_x} \sum_{n=-N}^{N-1} |x_a[n]|^2 e^{j\frac{\pi\lambda n}{\Delta_x}}, \quad -\Delta_x \leq \lambda < \Delta_x \quad (11)$$

where  $N$  is an arbitrary integer that is greater than  $\Delta_x^2$ , which is the time-bandwidth product  $\Delta_x^2$  of  $x_a(r)$ , and  $x_a[n] \triangleq x_a(n/2\Delta_x)$  is the  $n$ th sample of the FrFT  $x_a(r)$ . To obtain  $2N$  equally spaced radial samples of  $A_x^p(\lambda, \phi)$ , we substitute  $\lambda = (k/N)\Delta_x$  in the above equation:

$$A_x^p\left(\frac{k}{N}\Delta_x, \phi\right) = \frac{1}{2\Delta_x} \sum_{n=-N}^{N-1} |x_a[n]|^2 e^{j\frac{2\pi kn}{2N}} \quad -N \leq k \leq N-1. \quad (12)$$

After the discretization, the obtained form lends itself for an efficient digital computation since the required samples of the FrFT  $[x_a(n/2\Delta_x), -N \leq n \leq N-1]$  can be computed using the recently developed fast computation algorithm [36] in  $O(N \log N)$  flops. The summation in (12) can be recast into a  $2N$ -point discrete Fourier transformation (DFT), which can be computed in  $O(N \log N)$  flops using the fast Fourier transform algorithm. Therefore, the overall cost of computing the samples of the AF along any radial slice is  $O(N \log N)$  flops.

Note that the relationship in (12) is discrete in the radial variable  $k$  and continuous in the angular variable  $\phi$ . By discretizing the angular variable, the samples of the AF along several radial lines can be computed. For instance, if this algorithm is used for a uniformly distributed set of angles  $\phi_m = (\pi/M)k, 0 \leq k \leq M-1$ , covering the range  $[0, \pi)$ , then the samples of the AF located on a polar grid can be computed in  $O(MN \log N)$  flops. In Fig. 3(a), we illustrate the shape of a polar grid on which the samples of the AF  $A_x(\nu, \tau)$  can be computed by using this algorithm.

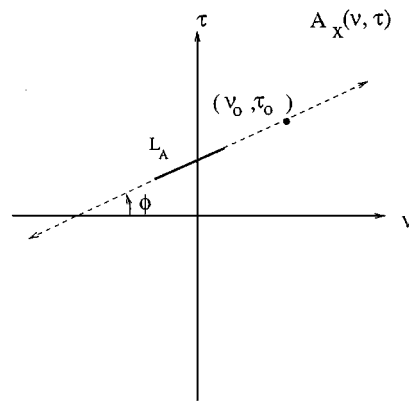


Fig. 2. Nonradial slice of the ambiguity function.

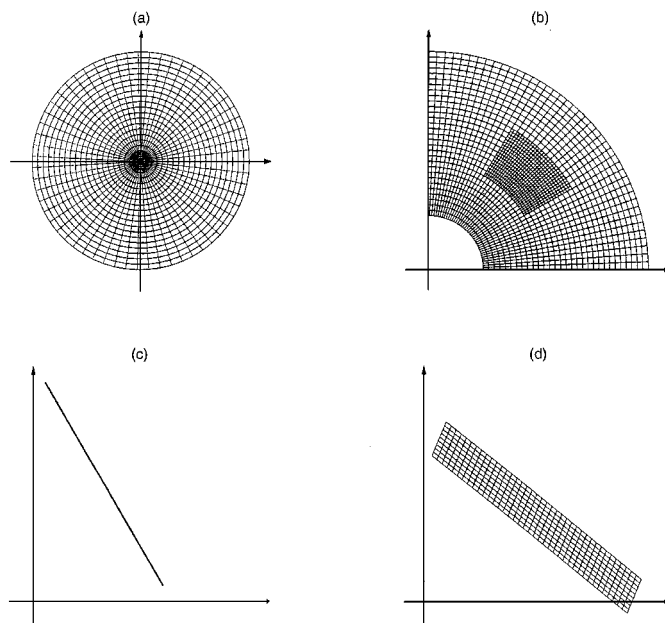


Fig. 3. Some grids on which the AF and/or WD of a signal can be computed. (a) Full polar grid. (b) Partial polar grid with nonuniform grid density. (c) Arbitrary line segment. (d) Parallelogram.

### C. Computation of the Ambiguity Function along the Segments of the Radial Slices

In order to compute the samples of the AF on an arbitrarily positioned segment of a radial slice, the chirp  $z$ -transform (CZT) algorithm [37] can be used. Here, we will use a special version of this algorithm (which is also called the chirp transform algorithm) to compute  $N'$  uniformly spaced samples of a radial slice  $A_x^p(\lambda, \phi)$  on the interval  $[\lambda_i, \lambda_f]_{\text{mod}(2\Delta_x)}$  for arbitrary values of the parameters  $N', \lambda_i$ , and  $\lambda_f$ .

To obtain the required samples, we substitute  $\lambda = \lambda_i + k\Delta_\lambda, 0 \leq k \leq N' - 1$  in (11), where the sampling interval of the frequency variable is  $\Delta_\lambda = (\lambda_f - \lambda_i)/(N' - 1)$ . After the rearrangement of the summation as

$$A_x^p(\lambda_i + k\Delta_\lambda, \phi) = \frac{1}{2\Delta_x} \sum_{n=-N}^{N-1} \left( |x_a[n]|^2 e^{j\pi\frac{\lambda_i}{\Delta_x}n} \right) e^{j\pi\frac{\Delta_\lambda}{\Delta_x}kn} \quad (13a)$$

<sup>2</sup>Complex multiplication and addition.

<sup>3</sup>From this observation, we deduce the following fact: If the WD of  $x(t)$  is confined into a circle with radius  $\Delta_x/2$  in the Wigner plane, then its AF is confined into a circle with radius  $\Delta_x$  in the ambiguity plane.

$$= \sum_{n=-N}^{N-1} g[n]W^{kn}, \quad k = 0, 1, \dots, N' - 1 \quad (13b)$$

where  $g[n]$  and  $W$  are defined as

$$g[n] = \frac{1}{2\Delta_x} |x_a[n]|^2 e^{j\pi \frac{\lambda_i}{\Delta_x} n} \quad (14)$$

$$W = e^{j\pi \frac{\Delta_\lambda}{\Delta_x}} \quad (15)$$

we use the identity  $kn = (1/2)[k^2 + n^2 - (k - n)^2]$  in (13b) and obtain an alternative but equivalent expression for  $A_x^p(\lambda_i + k\Delta_\lambda, \phi)$ :

$$A_x^p(\lambda_i + k\Delta_\lambda, \phi) = W^{k^2/2} \sum_{n=-N}^{N-1} W^{-(k-n)^2/2} \left( g[n]W^{n^2/2} \right) \quad k = 0, 1, \dots, N' - 1. \quad (16)$$

In this expression,  $A_x^p(\lambda_i + k\Delta_\lambda, \phi)$  can be interpreted as the convolution of the chirp-modulated signal  $g[k]$  and the chirp  $W^{-k^2/2}$  multiplied with another chirp  $W^{k^2/2}$ . Since the convolution can be computed efficiently by using the FFT algorithm, for the usual case of  $N' \leq N$ , the uniformly spaced samples of the radial slice  $A_x^p(\lambda, \phi)$  located in the segment  $[\lambda_i, \lambda_f]_{\text{mod}(2\Delta_x)}$  can be obtained in  $O(N \log N)$  flops. In Fig. 3(b), we illustrate the shape of a partial polar grid, on which the samples of the AF  $A_x(\nu, \tau)$  can be computed by using the algorithm of the previous section combined with the CZT algorithm. In this plot, the polar grid has denser samples in the middle region. The samples on the radial slices that pass through both the denser and nondenser parts of the grid can be obtained by using the CZT algorithm three times: once to compute the samples in the denser region and twice to compute the samples in the nondenser regions.

#### D. Computation of the Ambiguity Function Along Arbitrary Line Segments

In this section, we present a fast computational algorithm that computes the samples of AF on a nonradial slice. Let us consider the case of computing the samples of the AF  $A_x(\nu, \tau)$  along the line segment  $L_A$  shown in Fig. 2. The following parameterization for the line segment  $L_A$  will be used in the derivations:

$$L_A = \{(\nu, \tau) \mid \nu = \nu_o + \lambda \cos \phi, \tau = \tau_o + \lambda \sin \phi, \lambda_i \leq \lambda \leq \lambda_f\} \quad (17)$$

where  $(\nu_o, \tau_o)$  is an arbitrary point that lies on  $L_A$ , and  $\phi$  is the angle between  $L_A$  and the  $\nu$  axis. Using this parameterization of  $L_A$  and the definition of the AF, the nonradial slice of the AF that lies on the line segment  $L_A$  can be written as

$$A_x(\nu_o + \lambda \cos \phi, \tau_o + \lambda \sin \phi) = \int x \left( t + \frac{\tau_o + \lambda \sin \phi}{2} \right) \times x^* \left( t - \frac{\tau_o + \lambda \sin \phi}{2} \right) e^{j2\pi(\nu_o + \lambda \cos \phi)t} dt \quad (18a)$$

$$\equiv A_{yz}(\lambda \cos \phi, \lambda \sin \phi) \quad (18b)$$

where  $A_{yz}(\nu, \tau)$  is the cross-ambiguity function of the following time-domain signals  $y(t)$  and  $z(t)$ :

$$y(t) = x(t + \tau_o/2) e^{j\pi \nu_o t} \quad (19)$$

$$z(t) = x(t - \tau_o/2) e^{-j\pi \nu_o t}. \quad (20)$$

Thus, the nonradial slice of  $A_x(\nu, \tau)$  is equal to the radial slice of the  $A_{yz}(\nu, \tau)$ , where both of the slices are in parallel. Hence, similar to (8), the projection-slice theorem can be used to express the slice of the  $A_x(\nu, \tau)$  along the line segment  $L_A$  as the 1-D inverse FT of the  $\phi$ -Radon projection of the corresponding cross-Wigner distribution  $W_{yz}(t, f)$ :

$$A_x(\nu_o + \lambda \cos \phi, \tau_o + \lambda \sin \phi) = \int P_{yz}(r, \phi) e^{j2\pi r \lambda} dr. \quad (21)$$

We note that analogous to (9), the  $\phi$ -Radon projections of the cross WD can be obtained from the following FrFT relation [20]:

$$P_{yz}(r, \phi) = [\{\mathcal{F}^a y\}(r)][\{\mathcal{F}^a z\}(r)]^* \equiv y_a(r)z_a^*(r) \quad (22)$$

where  $a = 2\phi/\pi$  is the FrFT order. Then, following the discussions in Sections III-B and C, we obtain the following expression for the  $N'$  uniformly spaced samples of the AF on the line segment  $L_A$ :

$$A_x(\nu_o + \lambda_k \cos \phi, \tau_o + \lambda_k \sin \phi) = \frac{1}{2\Delta_x} \sum_{n=-N}^{N-1} y_a \left( \frac{n}{2\Delta_x} \right) z_a^* \left( \frac{n}{2\Delta_x} \right) e^{j\frac{\pi \lambda_k n}{\Delta_x}} \quad k = 0, 1, \dots, N' - 1 \quad (23)$$

where  $\lambda_k = \lambda_i + k((\lambda_f - \lambda_i)/(N' - 1))$ . As in the last section, these samples of the AF on the nonradial line segment  $L_A$  can be computed using the chirp transform algorithm.

#### IV. FAST COMPUTATION OF THE WIGNER DISTRIBUTION ON ARBITRARY LINE SEGMENTS

In the rest of this paper, we will present the dual development for the Wigner distribution. In the next section, we introduce the dual of the Radon-Wigner transform: the Radon-ambiguity function transform (RAFT). Then, we derive the relationship between the RAFT and FrFT. As in the computation of the AF samples, this relationship will naturally lead us to the fast computation algorithm for the required WD samples.

##### A. Radon-Ambiguity Transform

The Radon transformation has been found to be a useful tool in time-frequency signal processing with applications to detection of chirp rates [26] and signal-dependent kernel design [24]. As we show in the following sections, the Radon transform of the ambiguity function itself is also an important tool in the efficient computation of the WD slices.

Here, we introduce the Radon-ambiguity function transform of a signal  $y(t)$  as the Radon transform of its ambiguity function. The RAFT can be written as

$$Q_y(r, \phi) = \int A_y(r \cos \phi - s \sin \phi, r \sin \phi + s \cos \phi) ds \quad (24)$$

where  $(r, \phi)$  are the polar format variables. Using the projection-slice theorem, the radial slice of the WD at an angle  $\phi$  can be written as the FT of  $Q_y(r, \phi)$  with respect to the radial variable  $r$

$$\int Q_y(r, \phi) e^{-j2\pi r \lambda} dr = W_y(\lambda \cos \phi, \lambda \sin \phi) \quad (25a)$$

$$= W_y^P(\lambda, \phi) \quad (25b)$$

where  $W_y^P(\lambda, \phi) \triangleq W_y(\lambda \cos \phi, \lambda \sin \phi)$  is the polar representation of the WD.

To obtain a fast computational algorithm similar to that in Section III-B, the samples of the projections  $Q_y(r, \phi)$  have to be obtained efficiently. In the next section, we investigate the relationship between the RAFT and the FrFT.

### B. Relation Between the Radon-Ambiguity Function Transformation and the Fractional Fourier Transformation

The relationship of the RWT to the FrFT is well known in the literature. In this section, we show that a similar relationship exists between the RAFT and FrFT. We start with the substitution of (4b) into (24), resulting in the following expression for the radial slice of the RAFT:

$$Q_y(r, \phi) = \iint y(t + \tau/2) y^*(t - \tau/2) \times e^{j2\pi \nu t} \Big|_{\substack{\nu = r \cos \phi - s \sin \phi \\ \tau = r \sin \phi + s \cos \phi}} dt ds \quad (26a)$$

$$= \iint y \left( t + \frac{r \sin \phi + s \cos \phi}{2} \right) \times y^* \left( t - \frac{r \sin \phi + s \cos \phi}{2} \right) \times e^{j2\pi(r \cos \phi - s \sin \phi)t} dt ds. \quad (26b)$$

By making the following change in the integration variables:

$$\begin{bmatrix} t_1 \\ t_2 \end{bmatrix} = \begin{bmatrix} 1 & +\frac{1}{2} \cos \phi \\ 1 & -\frac{1}{2} \cos \phi \end{bmatrix} \begin{bmatrix} t \\ s \end{bmatrix} + \frac{1}{2} r \sin \phi \begin{bmatrix} 1 \\ -1 \end{bmatrix} \quad (27)$$

$$dt_1 dt_2 = |\cos \phi| dt ds \quad (28)$$

the integral in (26b) can be written as in the following separable form:

$$Q_y(r, \phi) = \iint y(t_1) y^*(t_2) e^{j\pi[-(t_1^2 - t_2^2) \tan \phi + (t_1 + t_2)r \sec \phi]} \times \frac{1}{|\cos \phi|} dt_1 dt_2. \quad (29)$$

By using the definition of  $A_\phi$  given in (56), it follows that  $1/|\cos \phi| = |A_{\phi - \pi/2} e^{-j\pi(r/2)^2 \tan \phi}|^2$ . After substituting this identity into (29), the separated terms can be written in the form of FrFT

$$Q_y(r, \phi) = \left[ \int A_{\phi - \pi/2} e^{j\pi(-(r/2)^2 \tan \phi + r t_1 \sec \phi - t_1^2 \tan \phi)} \times y(t_1) dt_1 \right] \times \left[ \int A_{\phi - \pi/2} e^{-j\pi((r/2)^2 \tan \phi + r t_2 \sec \phi + t_2^2 \tan \phi)} \times y(t_2) dt_2 \right]^* \quad (30a)$$

$$= \left[ \left\{ \mathcal{F}^{(a-1)} y \right\} (r/2) \right] \left[ \left\{ \mathcal{F}^{(a-1)} y \right\} (-r/2) \right]^* \quad (30b)$$

$$= y_{(a-1)}(r/2) y_{(a-1)}^*(-r/2) \quad (30c)$$

where  $(a - 1) = (2/\pi)\phi - 1$  is the FrFT order. Thus, combining (25) with (30) and discretizing the obtained relationship, we obtain an algorithm that can be used to compute the samples of the WD on polar grids, such as the ones shown in Figs. 3(a) and (b). In the following section, based on the above relationship, we propose an efficient algorithm to compute samples of the WD on arbitrary line segments.

### C. Computation of the Wigner Distribution along Arbitrary Line Segments

Suppose that we want to compute samples of the WD of a waveform  $x(t)$  along an arbitrary line segment  $L_W$  in the Wigner plane. Since the line segment  $L_W$  may not pass through the origin, we cannot immediately use the results of the previous section. However, as in Section III-D, we will express the required nonradial slice as the radial slice of the WD of another function that allows us to use the results of the previous section. In the following derivation, we parameterize the line segment  $L_W$  as

$$L_W = \{(t, f) | t = t_o + \lambda \cos \phi, f = f_o + \lambda \sin \phi, \lambda_i \leq \lambda \leq \lambda_f\}. \quad (31)$$

In this expression,  $(t_o, f_o)$  is an arbitrary point that lies on  $L_W$ , and  $\phi$  is the angle of  $L_W$  with the  $t$  axis. Using this parameterization of  $L_W$ , the nonradial slice of the WD can be expressed as

$$W_x(t_o + \lambda \cos \phi, f_o + \lambda \sin \phi) = \int x(t_o + \lambda \cos \phi + t'/2) x^*(t_o + \lambda \cos \phi - t'/2) \times e^{-j2\pi(f_o + \lambda \sin \phi)t'} dt' \quad (32a)$$

$$\equiv W_y(\lambda \cos \phi, \lambda \sin \phi) \quad (32b)$$

where  $W_y(\lambda \cos \phi, \lambda \sin \phi)$  is the radial slice of the WD of  $y(t)$ :

$$y(t) = x(t + t_o) e^{-j2\pi f_o t}. \quad (33)$$

Hence, the nonradial slice of the WD of  $x(t)$  is the same as the radial slice of the WD of the time-shifted and frequency-modulated version of it, where both slices are in parallel. By using the projection-slice theorem given in (25), the nonradial slice of the WD of  $x(t)$  can be obtained as

$$W_x(t_o + \lambda \cos \phi, f_o + \lambda \sin \phi) = \int Q_y(r, \phi) e^{-j2\pi r \lambda} \quad (34)$$

where  $Q_y(r, \phi)$  is the  $\phi$ -Radon projection of the ambiguity function  $A_y(\nu, \tau)$ . Since the required  $\phi$ -Radon projection satisfies the following FrFT relationship:

$$Q_y(r, \phi) = y_{(a-1)}(r/2) y_{(a-1)}^*(-r/2) \quad (35)$$

where  $a = 2\phi/\pi$ , it can be efficiently computed by using the fast FrFT algorithm proposed in [36] and given here as Algorithm 1. The steps of the proposed  $O(N \log N)$  algorithm are given in Algorithm 3. Note that unlike  $P_x(r, \phi)$ , which is the  $\phi$ -Radon

**Object of the algorithm:**

Given  $f(n/\Delta_x)$ ,  $-N/2 \leq n \leq N/2 - 1$ , to compute  $f_a(m/2\Delta_x)$ ,  $-N \leq m \leq N - 1$ , under the assumption that the WD of  $f(t)$  is confined into a circle with diameter  $\Delta_x \leq \sqrt{N}$ .

**Steps of the algorithm:**

Interpolate the input samples by 2:  $f(n/\Delta_x) \rightarrow f(n/2\Delta_x)$

$a' := (a + 2 \bmod 4) - 2$                       % After the modulo operation,  $a' \in [-2, 2)$

% The cases of  $|a'| \in [0.5, 1.5]$  and  $|a'| \notin [0.5, 1.5]$  have to be treated separately.

**if**  $|a'| \in [0.5, 1.5]$  **then**

$a'' := a'$

**else**

$a'' := (a' + 1 \bmod 4) - 2$                       % After the modulo operation,  $a'' \in (0.5, 1.5)$

**end if**

$\phi'' := \frac{\pi}{2} a''$

$\alpha'' := \cot \phi''$

$\beta'' := \csc \phi''$

$A_{\phi''} := \frac{\exp(-j\pi \operatorname{sgn}(\sin \phi'')/4 + j\phi''/2)}{|\sin \phi''|^{1/2}}$

    % Compute the following sequences:

$c_1[m] := e^{j\pi \frac{1}{4}(\alpha''/\Delta_x^2 - \beta''/N)m^2}$       for  $-N \leq m \leq N - 1$

$c_2[m] := e^{j\pi \beta''(m/2\sqrt{N})^2}$               for  $-2N \leq m \leq 2N - 1$

$c_3[m] := e^{j\pi \frac{\Delta_x^2}{4N}(\alpha''/N - \beta''/\Delta_x^2)m^2}$       for  $-N \leq m \leq N - 1$

$g[m] := c_1[m]f(m/2\Delta_x)$               for  $-N \leq m \leq N - 1$

$h_{a''}(m/2\Delta_x) := \frac{A_{\phi''}}{2\Delta_x} c_3[m](c_2 * g)[m]$       for  $-N \leq m \leq N - 1$

    %In the last step FFT is used to compute the convolution in  $O(N \log N)$  flops.

**if**  $|a'| \in [0.5, 1.5]$  **then**

$f_a(m/2\Delta_x) := h_{a''}(m/2\Delta_x)$

**else**

    % Compute samples of the ordinary FT using FFT.

$f_a(m/2\Delta_x) := \{\mathcal{F}^{-1}h_{a''}\}(m/2\Delta_x)$

**end if**

Algorithm 1. Fast fractional Fourier transform algorithm proposed in [36].

projection of the WD given by (7), the double-sided bandwidth of  $Q_y(r, \phi)$  is  $\Delta_x$ .

## V. FAST COMPUTATION OF THE CROSS AMBIGUITY FUNCTION AND THE CROSS WIGNER DISTRIBUTION ON ARBITRARY LINE SEGMENTS

Up to now, our main objective was developing algorithms for efficient computation of the samples of the AF and WD on arbitrary line segments. However, in some applications [14], [38], it is required to compute the cross AF and the cross WD of a pair of given signals. As we show below, the same algorithms, with some slight modifications, can still be used to compute samples of the cross AF and the cross WD on arbitrary line segments efficiently.

### A. Fast Computation of the Cross Ambiguity Function on Arbitrary Line Segments

Suppose that we want to compute the samples of the cross AF of the two signals  $y(t)$  and  $z(t)$  on the line segment  $L_A$  shown in Fig. 2. This nonradial slice of the cross AF function is given as

$$A_{yz}(\nu_o + \lambda \cos \phi, \tau_o + \lambda \sin \phi) = \int y\left(t + \frac{\tau_o + \lambda \sin \phi}{2}\right) z^*\left(t - \frac{\tau_o + \lambda \sin \phi}{2}\right) \times e^{j2\pi(\nu_o + \lambda \cos \phi)t} dt \quad (36a)$$

$$\equiv A_{\tilde{y}\tilde{z}}(\lambda \cos \phi, \lambda \sin \phi) \quad (36b)$$

**Object of the algorithm:**

Given  $y(n/\Delta_x)$  and  $z(n/\Delta_x)$ ,  $-N/2 \leq n \leq N/2 - 1$ , to compute  $N'$  samples of the cross AF of  $y(t)$  and  $z(t)$  along the line segment  $L_A$  as shown in Fig. 2.

**Steps of the algorithm:**

**if** a radial slice **then**

$$y_a[n] := \{\mathcal{F}^a y\}(n/2\Delta_x) \quad \text{for } -N \leq n \leq N-1 \quad \text{by using Algorithm 1.}$$

$$z_a[n] := \{\mathcal{F}^a z\}(n/2\Delta_x) \quad \text{for } -N \leq n \leq N-1 \quad \text{by using Algorithm 1.}$$

$$p_a[n] \triangleq P_{yz}(n/2\Delta_x, \phi) := y_a[n]z_a^*[n] \quad \text{for } -N \leq n \leq N-1$$

**else**

$$\tilde{y}[n] := y(n/\Delta_x + \tau_o/2)e^{j\pi\nu_o(n/\Delta_x)} \quad \text{for } -N/2 \leq n \leq N/2 - 1$$

$$\tilde{z}[n] := z(n/\Delta_x - \tau_o/2)e^{-j\pi\nu_o(n/\Delta_x)} \quad \text{for } -N/2 \leq n \leq N/2 - 1$$

$$\tilde{y}_a[n] := \{\mathcal{F}^a \tilde{y}\}(n/2\Delta_x) \quad \text{for } -N \leq n \leq N-1 \quad \text{by using Algorithm 1.}$$

$$\tilde{z}_a[n] := \{\mathcal{F}^a \tilde{z}\}(n/2\Delta_x) \quad \text{for } -N \leq n \leq N-1 \quad \text{by using Algorithm 1.}$$

$$p_a[n] \triangleq P_{\tilde{y}\tilde{z}}(n/2\Delta_x, \phi) := \tilde{y}_a[n]\tilde{z}_a^*[n] \quad \text{for } -N \leq n \leq N-1$$

**end if**

$$A_{yz}(\nu_k, \tau_k) := \frac{1}{2\Delta_x} \sum_{n=-N}^{N-1} p_a[n]e^{j\frac{\pi}{\Delta_x}\lambda_k n} \quad \text{for } 0 \leq k \leq N' - 1 \quad \text{by using the CZT Algorithm.}$$

where  $(\nu_k, \tau_k) \triangleq (\nu_o + \lambda_k \cos \phi, \tau_o + \lambda_k \sin \phi)$  and  $\lambda_k \triangleq \lambda_i + k\frac{\lambda_f - \lambda_i}{N' - 1}$ .

Algorithm 2. Fast computation of the cross-ambiguity function on arbitrary line segments.

**Object of the algorithm:**

Given  $y(n/\Delta_x)$  and  $z(n/\Delta_x)$ ,  $-N/2 \leq n \leq N/2 - 1$ , to compute  $N'$  samples of the cross WD of  $y(t)$  and  $z(t)$  along the line segment  $L_W$  as parameterized in (31).

**Steps of the algorithm:**

**if** a radial slice **then**

$$y_{(a-1)}[n] := \{\mathcal{F}^{(a-1)} y\}(n/2\Delta_x) \quad \text{for } -N \leq n \leq N-1 \quad \text{by using Algorithm 1.}$$

$$z_{(a-1)}[n] := \{\mathcal{F}^{(a-1)} z\}(n/2\Delta_x) \quad \text{for } -N \leq n \leq N-1 \quad \text{by using Algorithm 1.}$$

$$q_{(a-1)}[n] \triangleq Q_{yz}(n/\Delta_x, \phi) := y_{(a-1)}[n]z_{(a-1)}^*[-n] \quad \text{for } -N \leq n \leq N-1$$

**else**

$$\tilde{y}[n] := y(n/\Delta_x + t_o)e^{-j2\pi f_o(n/\Delta_x)}$$

$$\tilde{z}[n] := z(n/\Delta_x + t_o)e^{-j2\pi f_o(n/\Delta_x)}$$

$$\tilde{y}_{(a-1)}[n] := \{\mathcal{F}^{(a-1)} \tilde{y}\}(n/2\Delta_x) \quad \text{for } -N \leq n \leq N-1 \quad \text{by using Algorithm 1.}$$

$$\tilde{z}_{(a-1)}[n] := \{\mathcal{F}^{(a-1)} \tilde{z}\}(n/2\Delta_x) \quad \text{for } -N \leq n \leq N-1 \quad \text{by using Algorithm 1.}$$

$$q_{(a-1)}[n] \triangleq Q_{\tilde{y}\tilde{z}}(n/\Delta_x, \phi) := \tilde{y}_{(a-1)}[n]\tilde{z}_{(a-1)}^*[-n] \quad \text{for } -N \leq n \leq N-1$$

**end if**

$$W_{yz}(t_k, f_k) := \frac{1}{\Delta_x} \sum_{n=-N}^{N-1} q_{(a-1)}[n]e^{-j\frac{2\pi}{\Delta_x}\lambda_k n} \quad \text{for } 0 \leq k \leq N' - 1 \quad \text{by using CZT Algorithm.}$$

where  $(t_k, f_k) \triangleq (t_o + \lambda_k \cos \phi, f_o + \lambda_k \sin \phi)$  and  $\lambda_k \triangleq \lambda_i + k\frac{\lambda_f - \lambda_i}{N' - 1}$ .

Algorithm 3. Fast computation of the cross-Wigner distribution on arbitrary line segments.

where  $A_{\tilde{y}\tilde{z}}(\lambda \cos \phi, \lambda \sin \phi)$  is the radial slice of the cross AF of the signals  $\tilde{y}(t)$  and  $\tilde{z}(t)$ :

$$\tilde{y}(t) = y(t + \tau_o/2)e^{j\pi\nu_o t} \quad (37)$$

$$\tilde{z}(t) = z(t - \tau_o/2)e^{-j\pi\nu_o t}. \quad (38)$$

The radial slice of the  $A_{\tilde{y}\tilde{z}}(\nu, \tau)$  is the 1-D inverse FT of the  $\phi$ -Radon projection of the  $W_{\tilde{y}\tilde{z}}(t, f)$

$$A_{\tilde{y}\tilde{z}}(\lambda \cos \phi, \lambda \sin \phi) = \int P_{\tilde{y}\tilde{z}}(r, \phi)e^{j2\pi\lambda r} dr \quad (39)$$

where the  $\phi$ -Radon projection satisfies the following relation with the FrFTs of  $\tilde{y}(t)$  and  $\tilde{z}(t)$ :

$$P_{\tilde{y}\tilde{z}}(r, \phi) = \tilde{y}_a(r)\tilde{z}_a^*(r), \quad a = \frac{2}{\pi}\phi. \quad (40)$$

Then, the required nonradial slice of the  $A_{yz}(\nu, \tau)$  can be obtained as

$$A_{yz}(\nu_o + \lambda \cos \phi, \tau_o + \lambda \sin \phi) = \int \tilde{y}_a(r)\tilde{z}_a^*(r)e^{j2\pi\lambda r} dr. \quad (41)$$

Discretization of this expression yields the fast computational algorithm.

### B. Fast Computation of the Cross Wigner Distribution on Arbitrary Line Segments

In this section, we derive the algorithm for fast computation of the samples of the  $W_{yz}(t, f)$  on an arbitrary line segment  $L_W$  as parameterized in (31). This nonradial slice of the cross WD can be expressed as the radial slice of  $W_{\tilde{y}\tilde{z}}(t, f)$

$$\begin{aligned} W_{yz}(t_o + \lambda \cos \phi, f_o + \lambda \sin \phi) \\ = \int y(t_o + \lambda \cos \phi + t'/2)z^*(t_o + \lambda \cos \phi - t'/2) \\ \times e^{-j2\pi(f_o + \lambda \sin \phi)t'} dt' \end{aligned} \quad (42a)$$

$$\equiv W_{\tilde{y}\tilde{z}}(\lambda \cos \phi, \lambda \sin \phi) \quad (42b)$$

where the signals  $\tilde{y}(t)$  and  $\tilde{z}(t)$  are defined as

$$\tilde{y}(t) = y(t + t_o)e^{-j2\pi f_o t} \quad (43)$$

$$\tilde{z}(t) = z(t + t_o)e^{-j2\pi f_o t}. \quad (44)$$

Using the projection-slice theorem, this radial slice of the  $W_{\tilde{y}\tilde{z}}(t, f)$  can be expressed as the 1-D FT of the  $\phi$ -Radon projection  $Q_{\tilde{y}\tilde{z}}(r, \phi)$  of the  $A_{\tilde{y}\tilde{z}}(\nu, \tau)$

$$W_{\tilde{y}\tilde{z}}(\lambda \cos \phi, \lambda \sin \phi) = \int Q_{\tilde{y}\tilde{z}}(r, \phi)e^{-j2\pi\lambda r} dr \quad (45)$$

where the  $\phi$ -Radon projection is given in terms of the  $(a - 1)$ th-order FrFTs of the signals  $\tilde{y}(t)$  and  $\tilde{z}(t)$

$$Q_{\tilde{y}\tilde{z}}(r, \phi) = \tilde{y}_{(a-1)}(r/2)\tilde{z}_{(a-1)}^*(-r/2). \quad (46)$$

Finally, substituting (45) and (46) into (42) gives

$$\begin{aligned} W_{yz}(t_o + \lambda \cos \phi, f_o + \lambda \sin \phi) \\ = \int \tilde{y}_{(a-1)}(r/2)\tilde{z}_{(a-1)}^*(r/2)e^{-j2\pi\lambda r} dr. \end{aligned} \quad (47)$$

Discretization of this expression as in (23) yields the fast computational algorithm.

## VI. SIMULATIONS

In this section, by using simulations, we will investigate the performance of the proposed algorithms. For this purpose, we consider the signals with analytically known ambiguity functions and Wigner distributions. This way, we will be able to investigate the error due to discretization of the fractional Fourier transformation on the obtained samples. First, we will investigate the performance of Algorithm 2, which computes the samples of the ambiguity function on arbitrary line segments. In this simulation, we use a linear-frequency modulated chirp signal with a rectangular envelope  $x(t) = \text{rect}(t/T)e^{j\pi[at^2 + 2bt]}$ , where the  $\text{rect}(\cdot)$  function takes

the value 1 if its argument falls into the range  $[-T/2, T/2]$ ,  $a$  is the rate of the chirp, and  $b$  is its initial phase. The corresponding ambiguity function has the following closed-form expression:

$$\begin{aligned} A_x(\nu, \tau) = e^{j2\pi\tau b}(T - |\tau|) \text{sinc}((\nu + a\tau)(T - |\tau|)) \\ \times \text{rect}(\tau/2T). \end{aligned} \quad (48)$$

In the simulation performed here, the values of the parameters are chosen as  $T = 6$ ,  $a = -1/4$ , and  $b = 1$ . Then, by sampling  $x(t)$  at a rate  $\Delta_x = 14$ , we obtained  $N = 196$  uniformly spaced samples in the interval  $[-\Delta_x/2, \Delta_x/2]$ . Since the significant energy of the  $a$ th-order FrFTs of  $x(t)$  are confined into this interval, no scaling is applied to the continuous time signal  $x(t)$ . In other words, the value of the scaling parameter is given as  $s = 1$ , which is also true for the other simulations in this section. In Fig. 4(a), Algorithm 2 is used to compute the AF samples on the full polar grid with the angular spacing of  $\pi/85$  rad and radial spacing of  $\Delta_x/210$  normalized units. As shown in Fig. 4(b), by using the same algorithm, samples of the AF can also be obtained over a partial polar grid with the same angular and radial sampling intervals. For the display purpose, the AF of the same signal could also be computed on a Cartesian grid. In this simulation, the AF is first computed by using the algorithm in [18] on the whole Cartesian grid with Doppler and delay spacings of  $1/\Delta_x$  units. Then, in Fig. 4(c), real parts of the computed AF samples that reside on a circular disk with radius 3 are plotted. To investigate the accuracy of the proposed algorithm, we computed in  $O(N \log N)$  flops the samples of the ambiguity function of the same chirp pulse over the radial line segment shown in Fig. 4(d). The real parts of the computed samples and their deviation from the samples computed by using (48) are shown in Fig. 4(e) and (f), respectively. As it can be seen from this example, the computed samples are highly accurate. Alternatively, the samples on the line segment shown in Fig. 4(d) could be approximated from the computed AF samples on the Cartesian grid by using a crude interpolator such as the nearest neighbor interpolator. The result of this alternative approach is shown in Fig. 4(g), where the real parts of the computed samples are plotted. With the comparison of the approximation errors in Fig. 4(f) and (h), it becomes apparent that the new algorithm produces a ten-times more accurate result for this simulation. Furthermore, when the line segment has arbitrary orientation with  $O(N)$  samples on it, the alternative computation based on the Cartesian grid requires  $O(N^2 \log N)$  flops. On the other hand, by using Algorithm 2, the same AF samples can be computed with ten times more accuracy in only  $O(N \log N)$  flops.

Next, we investigate the accuracy of the algorithms in computing the WD of the Gaussian pulse  $x(t) = 2^{1/4}e^{-\pi t^2}$ , which has the Wigner distribution

$$W(t, f) = 2e^{-2\pi(t^2 + f^2)}. \quad (49)$$

By sampling  $x(t)$  at a rate  $\Delta_x = 10\sqrt{2}$ , we obtained  $N = 200$  uniformly spaced samples in the interval  $[-\Delta_x/2, \Delta_x/2]$ . Fig. 5(a) and (b) are obtained by repeated application of the Algorithm 3. In (a), the WD is computed over a full, and in (b), it is computed over a partial polar grid. For the purpose of comparison, the WD samples are also computed on a Cartesian grid by using the algorithm in [1] with a sampling interval of



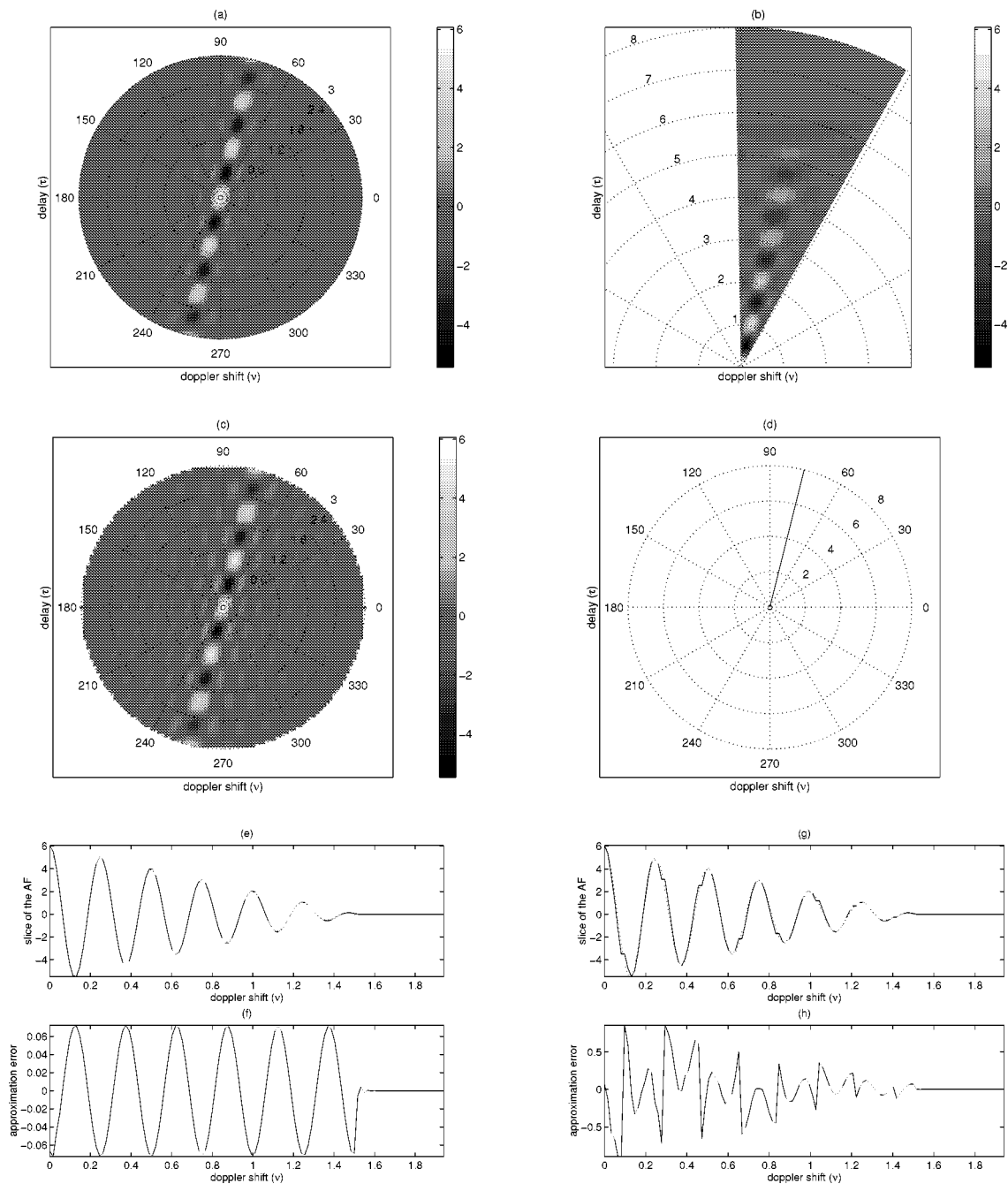


Fig. 4. Digital computation of the AF of a chirp signal with a rectangular envelope: In the top two plots, the real part of the AF of the pulse is computed on (a) full and (b) partial polar grid by repeated use of the Algorithm 2. For the purpose of comparison, the AF samples are also computed on a Cartesian grid by using [18]. In (c), the real parts of these AF samples that lie on a circular disk are plotted. In (d), the support of a radial line segment on which the samples of the AF are computed is shown. The real parts of the actual and computed AF samples on this line segment by using Algorithm 2 are in very good agreement, as shown by the close overlay in (e). The error in the computation shown in (f) reveals the highly accurate nature of the computational algorithm. In (g), the same AF samples are approximated from the samples on the Cartesian grid by using nearest neighbor interpolation. The peak approximation error in (h) is approximately ten times larger than the one in (f).

$1/(2\Delta_x)$  units both in time and frequency. Then, in Fig. 5(c), only the WD samples that lie on a circular disk with radius 1 are plotted.

To show the accuracy of the proposed algorithm, we computed, in  $O(N \log N)$  flops, samples of the Wigner distribution of the same Gaussian pulse over the nonradial line segment shown in Fig. 5(d). The obtained samples and the approximation error are plotted in Fig. 5(e) and (f), respectively. For the purpose

of comparison, the same AF samples are approximated from the Cartesian grid samples by using nearest neighbor interpolation. In Fig. 5(g), the approximated and actual AF samples are shown, and in Fig. 5(h), the computation error is shown. As in the AF case presented above, not only the accuracy of the computed samples shown in Fig. 5(h) is significantly less than the accuracy obtained by using Algorithm 3, but also the computation of the Cartesian grid based algorithm requires  $O(N^2 \log N)$  flops.

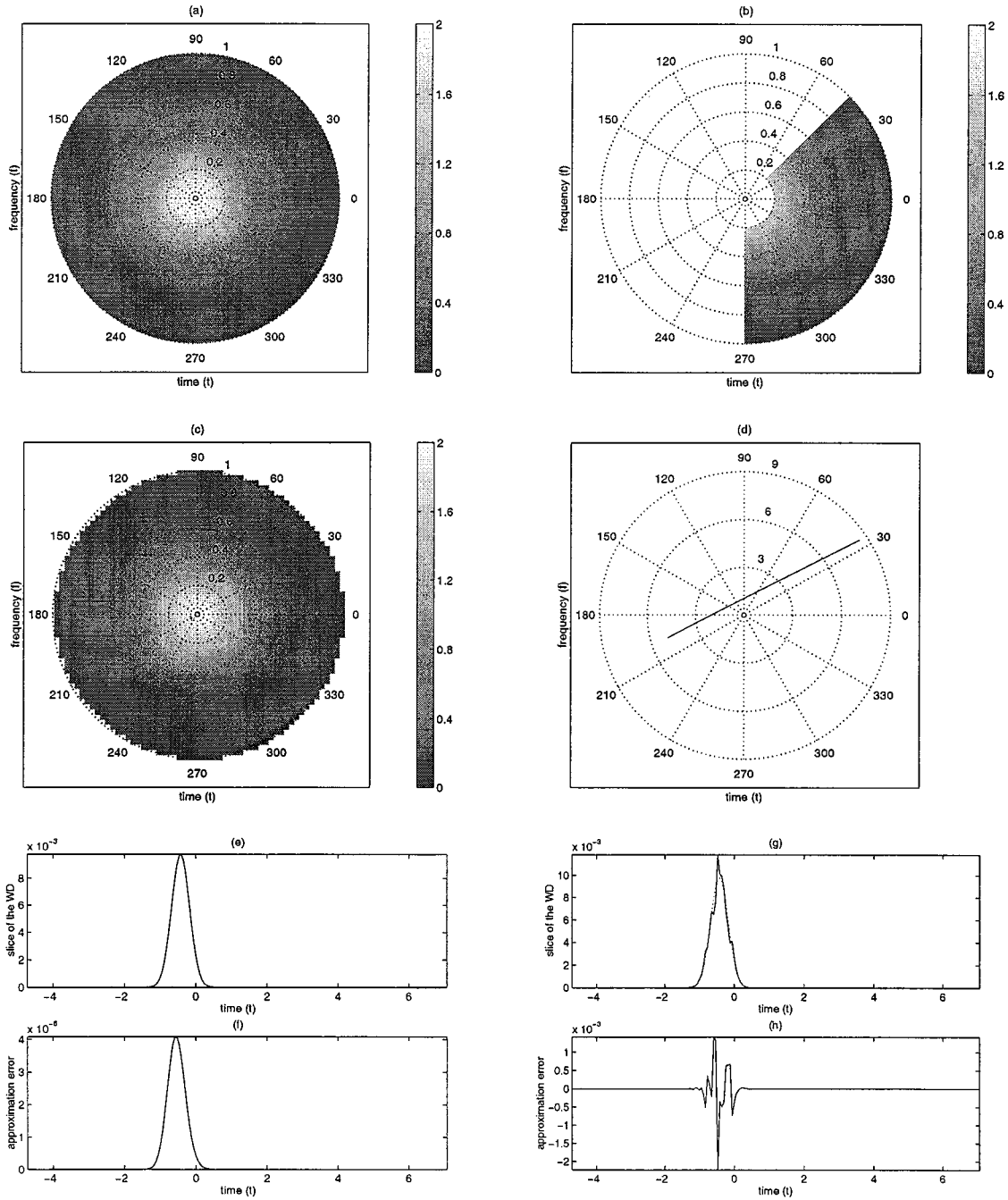


Fig. 5. Digital computation of the WD of a Gaussian pulse. In the top two plots, the WD of the pulse is computed on (a) full and (b) partial polar grid by repeated use of Algorithm 3. For the purpose of comparison, the WD samples are also computed on a Cartesian grid by using [1]. In (c), only the WD samples that lie on a circular disk are plotted. In (d), the support of a nonradial line segment on which the samples of the WD are computed is shown. The actual and computed WD samples on this line segment are in very good agreement, as shown by the close overlay in (e). The error in the computation shown in (f) reveals the highly accurate nature of the computational algorithm. In (g), the same WD samples are approximated from the samples on the Cartesian grid by using nearest neighbor interpolation. The error shown in (h) is significantly larger than the one in (f).

Next, we consider the digital computation of the WD of a multicomponent signal  $x(t)$ , which is composed of two chirp pulses  $x_1(t)$  and  $x_2(t)$ :

$$x(t) = x_1(t) + x_2(t). \quad (50)$$

The chirp pulses are chosen as

$$x_k(t) = e^{j\pi[a(t-t_o)^2 + 2b_k(t-t_o)]} \text{rect}((t-t_o)/T) \quad (51)$$

for  $k = 1$  or  $2$ . The WD of  $x(t)$  can be analytically computed as

$$\begin{aligned} W_x(t, f) = & W_r(t-t_o, f-at-b_1) \\ & + W_r(t-t_o, f-at-b_2) \\ & + 2 \cos(2\pi(b_2-b_1)(t-t_o)) \\ & \times W_r(t-t_o, f-at-(b_1+b_2)/2) \end{aligned} \quad (52)$$

where  $W_r(t, f)$  is the WD of the  $\text{rect}(t/T)$  function

$$\begin{aligned} W_r(t, f) = & 2T(1-2|t|/T) \text{rect}(t/T) \\ & \times \text{sinc}(2(1-2|t|/T)fT). \end{aligned} \quad (53)$$

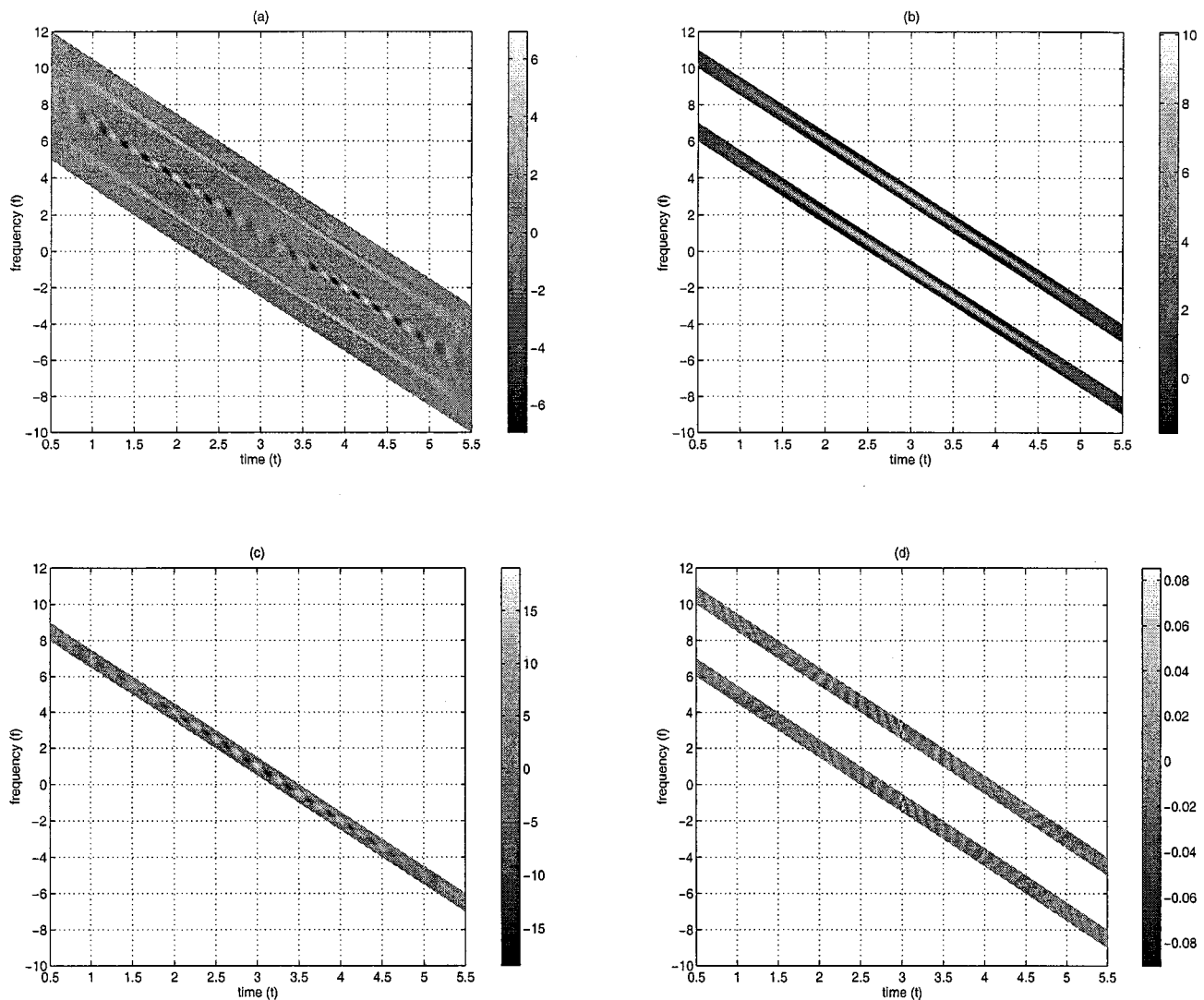


Fig. 6. Computation of the WD samples of a multicomponent chirp signal over various parallelogram grids to investigate the (a) whole, (b) auto and (c) cross terms. The efficient computation of the highly localized samples of the WD as in plots (b) and (c) has a wide range application areas including component analysis, signal detection, and signal extraction for nonstationary signals. As shown in (d), the error in the computed samples of the auto terms is very small.

In (52), the first two terms are the auto terms, and the third one is the cross term.

For the reported simulation here, the parameters of  $x(t)$  are chosen as  $\Delta_x = 30$ ,  $a = -3$ ,  $b_1 = 3$ ,  $b_2 = -1$ ,  $t_o = 3$ , and  $T = 5 + 1/\Delta_x$ . The WD of  $x(t)$  with these parameters is digitally computed on a grid like the one in Fig. 3(d) by using Algorithm 3. The obtained result shown in Fig. 6(a) demonstrates the agreement with the analytical result in (52). In this plot, we easily identify the auto terms of the WD as the two lines that are closer to the edges, and we identify the cross term as the line that is at the middle part of the plot. The cross term is highly oscillatory because of the cosine modulation in (52). In Fig. 6(b) and (c), computed samples of the auto and cross terms are shown over highly localized grids of the type given in Fig. 3(d). Finally, in Fig. 6(d), we provide the approximation error for the auto terms only.

In Fig. 7, the Radon-Wigner transform and Radon-ambiguity function transform of the same multicomponent signal are computed on polar grids by using the FrFT relations (9) and (30). These transforms have important applications in signal detec-

tion, multicomponent signal analysis, and data-adaptive kernel design for time-frequency signal analysis. The locations of the peaks in the RWT are related to the rate and initial phase of the chirps in (51). When the chirp components are contaminated with additive white Gaussian noise, the locations of the peaks in the Radon-Wigner transform provide the maximum likelihood estimate of these parameters [32], [39]. Note that the computation of the RWT and the RAFT of a signal over a full polar grid requires the computation of the same set of FrFTs of the signal. Hence, when these transforms are to be calculated simultaneously, significant computational savings can be achieved by avoiding any extra computation of the FrFT samples.

## VII. CONCLUSION

By using the FrFT of the time-domain signals, closed-form expressions for the projections of their auto or cross ambiguity functions are derived. Based on a similar formulation for the projections of the auto and cross Wigner distributions and the well-known 2-D Fourier transformation relationship between

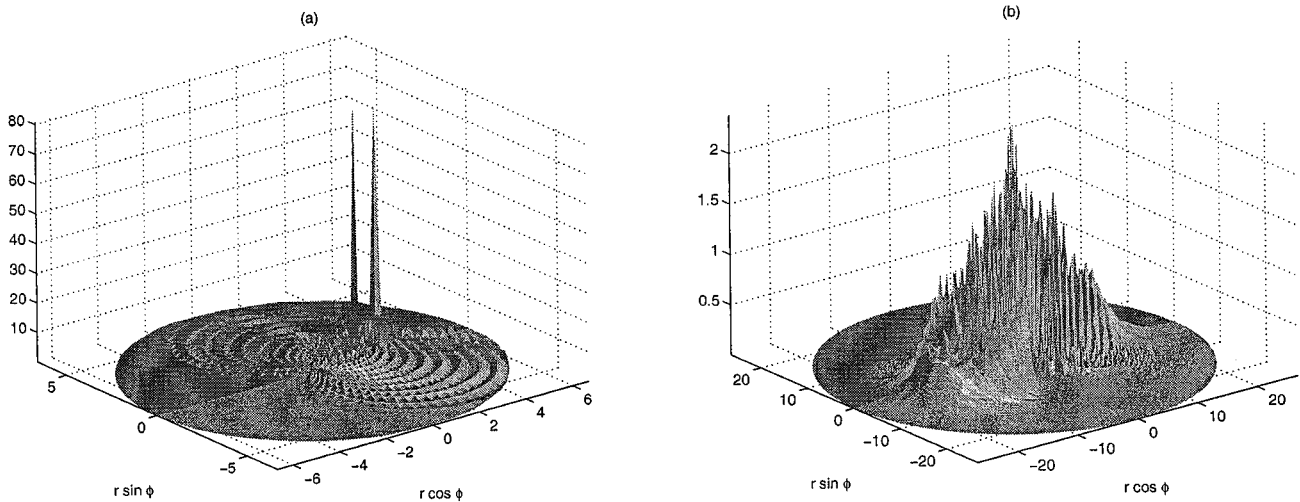


Fig. 7. Digital computation of the (a) Radon-Wigner transform and (b) magnitude of the Radon-ambiguity function transform. In this paper, the computation of these transforms constitute the intermediate steps in computation of the ambiguity function and the Wigner distribution on polar grids.

the ambiguity and Wigner domains, closed-form expressions are obtained for the slices of both the Wigner distribution and the ambiguity function. Based on the obtained analytical results, efficient algorithms are proposed for the computation of the auto or cross Wigner distribution and ambiguity function samples on arbitrary line segments. The proposed algorithms make use of a digital computation algorithm of the FrFT to compute  $N$  uniformly spaced samples in  $O(N \log N)$  flops. The ability of obtaining samples on arbitrary line segments provides significant flexibility in the computational applications involved with the Wigner distribution and the ambiguity function.

#### APPENDIX A

##### FRACTIONAL FOURIER TRANSFORMATION

The  $a$ th-order,  $a \in \mathfrak{R}$ ,  $0 < |a| < 2$ , FrFT of a function  $x(t)$  is defined as [40]

$$x_a(t) \triangleq \{\mathcal{F}^a x\}(t) \triangleq \int B_a(t, t') x(t') dt' \quad (54)$$

where the kernel of the transformation  $B_a(t, t')$  is

$$B_a(t, t') = A_\phi \exp[j\pi(t^2 \cot \phi - 2tt' \csc \phi + t'^2 \cot \phi)] \quad (55)$$

$$A_\phi = \frac{\exp(-j\pi \operatorname{sgn}(\sin \phi)/4 + j\phi/2)}{|\sin \phi|^{1/2}} \quad (56)$$

$$\phi = \frac{a\pi}{2}. \quad (57)$$

The transformation kernel is the complex exponential  $e^{-j2\pi t t'}$  for  $a = 1$ , and it approaches  $\delta(t)$  for  $a = 0$  and to  $\delta(t + t')$  for  $a = \pm 2$ . Thus, it follows that the first-order FrFT is the ordinary Fourier transform, and the zeroth-order FrFT is the function itself. The definition of the FrFT is easily extended to outside the interval  $[-2, 2]$  by noting that  $\mathcal{F}^{4k}$  is the identity operator for any integer  $k$  and the FrFT is additive in the index, i.e.,  $\mathcal{F}^{a_1} \mathcal{F}^{a_2} = \mathcal{F}^{a_1+a_2}$ .

#### REFERENCES

- [1] T. A. C. M. Claassen and W. F. G. Mecklenbrauker, "The Wigner distribution—A tool for time-time frequency signal analysis, part II: Discrete-time signals," *Philips J. Res.*, vol. 35, no. 4/5, pp. 276–350, 1980.
- [2] T. A. C. Claassen and W. F. G. Mecklenbrauker, "The aliasing problem in discrete-time Wigner distributions," *IEEE Trans. Acoust., Speech, Signal Processing*, vol. ASSP-31, pp. 1067–1072, Oct. 1983.
- [3] G. F. Boudreaux-Bartels and T. W. Parks, "Time-varying filtering and signal estimation using Wigner distribution synthesis techniques," *IEEE Trans. Acoust., Speech, Signal Processing*, vol. ASSP-34, pp. 442–451, June 1986.
- [4] L. Cohen, "Time-frequency distributions—A review," *Proc. IEEE*, vol. 77, pp. 941–981, July 1989.
- [5] F. Hlawatsch and G. F. Boudreaux-Bartels, "Linear and quadratic time-frequency signal representations," *IEEE Signal Processing Mag.*, vol. 9, pp. 21–67, Apr. 1992.
- [6] W. F. G. Mecklenbrauker, Ed., *The Wigner Distribution—Theory and Applications in Signal Processing*. New York: Elsevier, 1992.
- [7] L. R. Dragonette, D. M. Drumheller, C. F. Gaumont, D. H. Hughes, B. T. O'connor, N. Yen, and T. J. Yoder, "The application of two-dimensional signal transformations to the analysis and synthesis of structural excitations observed in acoustical scattering," *Proc. IEEE*, vol. 84, pp. 1249–1263, Sept. 1996.
- [8] P. K. Kumar and K. M. M. Prabhu, "Simulation studies of moving-target detection: A new approach with Wigner-Ville distribution," *Proc. Inst. Elect. Eng., Radar, Sonar Navig.*, vol. 144, no. 5, pp. 259–265, Oct. 1997.
- [9] S. Haykin and D. J. Thomson, "Signal detection in nonstationary environment reformulated as an adaptive pattern classification problem," *Proc. IEEE*, vol. 86, pp. 2325–2344, Nov. 1998.
- [10] V. Katkovnik and L. Stankovic, "Instantaneous frequency estimation using the Wigner distribution with varying data-driven window length," *IEEE Trans. Signal Processing*, vol. 46, pp. 3215–3225, Sept. 1998.
- [11] P. Flandrin, "Some features of time-frequency representations of multicomponent signals," in *Proc. IEEE Int. Conf. Acoust., Speech, Signal Process.*, vol. 3, 1984, pp. 41B.4.1–41B.4.4.
- [12] P. Bonato, A. Destefano, and R. Ceravolo, "Time-frequency and ambiguity function approaches in structural identification," *ASCE J. Eng. Mech.*, vol. 123, no. 12, pp. 1260–1267, 1997.
- [13] S. Parsons, C. W. Thorpe, and S. M. Dawson, "Echolocation calls of the long-tailed bat—A quantitative analysis of types of calls," *J. Mammol.*, vol. 78, no. 3, pp. 946–976, 1997.
- [14] P. M. Woodward, *Probability and Information Theory, with Applications to Radar*. New York: Pergamon, 1953.
- [15] C. H. Wilcox, "The synthesis problem for radar ambiguity functions," MRC Tech. Summary Rep. 157, Apr. 1960.
- [16] R. E. Blahut, W. Miller, and C. H. Wilcox Jr., *Radar and Sonar*. New York: Springer-Verlag, 1991, vol. 32.
- [17] G. C. Gaunard and H. C. Strifors, "Signal analysis by means of time-frequency (Wigner-type) distributions—Applications to sonar and radar echos," *Proc. IEEE*, vol. 84, pp. 1231–1248, Sept. 1996.

- [18] S. M. Sussman, "Least-squares synthesis of radar ambiguity functions," *IRE Trans. Inform. Theory*, vol. IT-8, pp. 246–254, Apr. 1962.
- [19] G. S. Cunningham and W. J. Williams, "Fast implementations of generalized discrete time-frequency distributions," *IEEE Trans. Signal Processing*, vol. 42, pp. 1496–1508, June 1994.
- [20] I. Raveh and D. Mendlovic, "New properties of the Radon transform of the cross Wigner/ambiguity distribution function," *IEEE Trans. Signal Processing*, vol. 47, pp. 2077–2080, July 1999.
- [21] R. G. Baraniuk and D. L. Jones, "A signal-dependent time-frequency representation: Optimal kernel design," *IEEE Trans. Signal Process.*, vol. 41, pp. 1589–1601, Apr. 1993.
- [22] —, "A signal-dependent time-frequency representation: Fast algorithm for optimal kernel design," *IEEE Trans. Signal Processing*, vol. 42, pp. 134–146, Jan. 1994.
- [23] —, "An adaptive optimal-kernel time-frequency representation," *IEEE Trans. Signal Process.*, vol. 43, pp. 2361–2371, Oct. 1995.
- [24] B. Ristic and B. Boashash, "Kernel design for time-frequency signal analysis using the Radon transform," *IEEE Trans. Signal Processing*, vol. 41, pp. 1996–2008, May 1993.
- [25] S. Barbarossa, "Analysis of multicomponent LFM signals by a combined Wigner-Hough transform," *IEEE Trans. Signal Processing*, vol. 43, pp. 1511–1515, June 1995.
- [26] M. Wang, A. K. Chan, and C. K. Chui, "Linear frequency-modulated signal detection using Radon-ambiguity transform," *IEEE Trans. Signal Processing*, vol. 46, pp. 571–586, Mar. 1998.
- [27] M. T. Ozgen and K. Demirbas, "Cohen's bilinear class of shift-invariant space/spatial-frequency signal representations for particle-location analysis of in-line Fresnel holograms," *J. Opt. Soc. Amer. A*, vol. 15, no. 8, pp. 2117–2137, Aug. 1998.
- [28] M. T. Ozgen, "An automatic kernel design procedure for the Cohen's bilinear class of representations as applied to in-line Fresnel holograms", submitted for publication.
- [29] L. Cohen, *Time-Frequency Analysis*. Englewood Cliffs, N.J.: Prentice-Hall, 1995.
- [30] J. C. Wood and D. T. Barry, "Tomographic time-frequency analysis and its application toward time-varying filtering and adaptive kernel desing for multicomponent linear-FM signals," *IEEE Trans. Signal Processing*, vol. 42, pp. 2094–2104, Aug. 1994.
- [31] —, "Linear sinal synthesis using the Radon-Wigner transform," *IEEE Trans. Signal Processing*, vol. 42, pp. 2105–2111, Aug. 1994.
- [32] —, "Radon transformation of time-frequency distributions for analysis of multicomponent signals," *IEEE Trans. Signal Processing*, vol. 42, pp. 3166–3177, Nov. 1994.
- [33] Z. Bao, G. Wang, and L. Luo, "Inverse synthetic aperture radar imaging of maneuvering targets," *Opt. Eng.*, vol. 37, no. 5, pp. 1582–1588, May 1998.
- [34] R. N. Bracewell, *Two-Dimensional Imaging*. Englewood Cliffs, NJ: Prentice-Hall, 1995.
- [35] A. W. Lohmann and B. H. Soffer, "Relationships between the Radon-Wigner and fractional Fourier transforms," *J. Opt. Soc. Amer. A*, vol. 11, pp. 1798–1801, 1994.
- [36] H. M. Ozaktas, O. Arikan, M. A. Kutay, and G. Bozdagi, "Digital computation of the fractional Fourier transform," *IEEE Trans. Signal Processing*, vol. 44, pp. 2141–2150, Sept. 1996.
- [37] L. R. Rabiner, R. W. Schafer, and C. M. Rader, "The chirp  $z$ -transform algorithm and its applications," *Bell Syst. Tech. J.*, vol. 48, pp. 1249–1292, May 1969.
- [38] T. J. McHale and G. F. Boudreaux-Bartels, "An algorithm for synthesizing signals from partial time-frequency models using the cross Wigner distribution," *IEEE Trans. Signal Processing*, vol. 41, pp. 1986–1990, May 1993.
- [39] S. Kay and G. F. Boudreaux-Bartels, "On the optimality of the Wigner distribution for detection," in *Proc. IEEE Int. Conf. Acoust. Speech, Signal Process.*, vol. 3, Mar. 1985, pp. 1017–1020.
- [40] V. Namias, "The fractional order Fourier transform and its application to quantum mechanics," *J. Inst. Math. Appl.*, vol. 25, pp. 241–265, 1980.



**Ahmet Kemal Özdemir** (S'97) was born in 1974 in Ankara, Turkey. He received the B.Sc. and M.S. degrees in electrical and electronics engineering from Bilkent University, Ankara, in 1996 and 1998, respectively. During his M.S. study, he was a Teaching and Research Assistant. He is currently pursuing the Ph.D. degree under the supervision of O. Arikan with the Department of Electrical and Electronics Engineering, Bilkent University.

His research interests are in digital signal processing and its applications to time-frequency analysis, radar signal processing, and communications.



**Orhan Arikan** (M'91) was born in 1964 in Manisa, Turkey. He received the B.Sc. degree in electrical and electronics engineering from the Middle East Technical University, Ankara, Turkey, in 1986 and both the M.S. and Ph.D. degrees in electrical and computer engineering from the University of Illinois, Urbana-Champaign, in 1988 and 1990, respectively.

Following his graduate studies, he worked for three years as a Research Scientist at Schlumberger-Doll Research, Ridgefield, CT. During this time, he was involved in the inverse problems and fusion of measurements with multiple modality. He joined Bilkent University, Ankara, in 1993, where he is presently Associate Professor of electrical engineering. His current research interests are in adaptive signal processing, time-frequency analysis, inverse problems, and array signal processing.

Dr. Arikan is the acting chairman of IEEE Turkey Section.